

Multiple ionization of neon atoms in collisions with bare and dressed ions: A mean-field description considering target response

Gerald Schenk* and Tom Kirchner†

Department of Physics and Astronomy, York University, Toronto, Ontario M3J 1P3, Canada

(Received 6 April 2015; published 29 May 2015)

We investigate projectile-charge-state-differential electron removal from neon atoms by impact of He^{2+} , Li^{3+} , B^{2+} , and C^{3+} ions at intermediate projectile energies (25 keV/u to 1 MeV/u). The many-electron problem is described with an independent electron model in which active electrons at both collision centers are propagated in a common mean-field potential. Response to electron removal is taken into account in terms of a time-dependent screening potential, and a Slater-determinant-based method is used for the final-state analysis. Total cross sections for net recoil ion production, multiple ionization, and capture channels are mostly in good agreement with published experimental data. Results from equicharged bare and dressed ions are compared and the net recoil ion production cross section is broken down into contributions associated with different final projectile charge states in order to shed light on the role of the projectile electrons.

DOI: [10.1103/PhysRevA.91.052712](https://doi.org/10.1103/PhysRevA.91.052712)

PACS number(s): 34.50.Fa, 34.70.+e

I. INTRODUCTION

The theoretical description of target electron removal in collisions with dressed projectiles, i.e., projectile ions that are not fully stripped of electrons, is more involved than for bare-ion collisions. One reason is that projectile electrons can be removed or transferred and thus change the final charge states. Calculations that take this into account and distinguish coincident charge states of fluorine-ion projectiles in impact ionization of neon were reported in Ref. [1], using a many-body extension of the classical-trajectory Monte Carlo (CTMC) [2] method. When an active role of projectile electrons is not considered, one faces the question of how to model the screening effect associated with passive electrons. A simple way of dealing with this is to approximate the total projectile potential by a Coulomb potential with an effective charge. Examples for such an effective potential approach are found in CTMC [2] and classical-trajectory eikonal calculations [3], where the choice of the effective potential is informed by spectroscopic energy-level data or by integrating the charge density of hydrogenlike wave functions up to the adiabatic radius of the outermost orbital [4].

A more involved method is to approximate screening by a charge that is a function of distance. This allows for incorporation of the correct asymptotic behavior of the projectile potential. Often parametric model potentials are used, for example, in perturbation theory [5] and in CTMC calculations [6,7]. Modeling the spatial dependence of the screening potential is conceptually straightforward in descriptions where the independent electron model (IEM) is used to approach the many-electron problem. Parametric potentials have been used to model target and projectile effective potentials in continuum distorted-wave with eikonal initial-state (CDW-EIS) calculations [8–11]. In Refs. [12–15] target and projectile effective potentials calculated with a density functional theory (DFT) approach have been used with the basis generator method (BGM) for orbital propagation [16]. Starting from

a parametric projectile potential, Ref. [17] developed for the CDW-EIS method an effective potential that is a function of the transferred momentum. Calculations for He^+ impact on noble gases [18,19] and B^{2+} impact on Ne [20] were based on this approach.

Recent experiments provided projectile-charge-state-coincident multiple ionization and charge transfer total cross sections for dressed-ion–atom collisions over a wide energy range [15,20–27]. In Ref. [20] so-called pure ionization channels (i.e., target ionization coincident with an unchanged projectile charge state) were published for the B^{2+} -Ne collision system. These experiments motivated us to investigate the role active projectile electrons have in such collisions [28]. We compared results of two-center BGM (TC-BGM) [29] calculations considering active target and projectile electrons, and calculations with passive projectile electrons only, with experimental data [20]. It was found that transfer ionization processes and coincident projectile ionization have a noticeable effect on pure ionization cross sections and calculations considering active projectile electrons are in better agreement with the experiments. Subsequently, we compared the active-electron results with a He^{2+} -Ne calculation using the same method to further explore the role of projectile electrons [30]. Of particular interest was that the net recoil ion production by bare-ion impact exceeds that of dressed-ion impact. In both works we noted it would be desirable to take time-dependent screening effects into account. Accordingly, in the present paper we investigate dressed-ion collisions with active electrons at target and projectile considering target response. We extract cross sections for more collision channels than in the previous work and also look into the C^{3+} -Ne system for which experimental data have become available very recently [26]. For both B^{2+} -Ne and C^{3+} -Ne cases, results are compared to those of equicharged bare ions in order to provide further insights into the role of projectile electrons in collisions.

The article is organized as follows: In Sec. II, we briefly explain our approach based on the TC-BGM. First, the effective potentials and their asymptotic requirements in the no-response approximation are introduced in Sec. II A. This is extended to encompass a time-dependent effective potential that models target response in Sec. II B. In order

*gschenk@yorku.ca

†tomk@yorku.ca

to establish terminology and the parameters used in the present calculations a brief overview of the BGM is given in Sec. II C. The theory section ends with an explanation of the statistical method used in the final-state analysis (Sec. II D). The nomenclature and definitions of the total cross sections that are compared in the following are also introduced in this section. Section III A compares no-response and target-response model results. Given that the response model can be viewed as a systematic improvement and since the response results are in better overall agreement with the experimental data, we focus on these calculations henceforth. Dressed- and bare-ion impacts on neon are compared for B^{2+} and He^{2+} projectiles in Sec. III B and for C^{3+} and Li^{3+} projectiles in Sec. III C. Both sections are structured in a similar way: Total cross sections for the net recoil ion production are presented first, followed by a discussion of the projectile-charge-state-coincident contributions to it. We explain the difference of net recoil ion production cross sections of the dressed and the bare projectiles based on these charge-state-coincident cross sections, comprising pure target ionization, transfer ionization, and (for the dressed projectiles) electron removal from both target and projectile. Total cross sections for single- and double-electron capture into the projectile are also compared with experimental results. The article closes with some concluding remarks in Sec. IV. Unless stated otherwise, atomic units are used throughout.

II. THEORY

We are investigating collisions that are fast enough to describe the motion of the nuclei by a straight-line trajectory. This reduces the scattering problem to a time-dependent Schrödinger equation for the N -electron dynamics, which depend on the parameters projectile kinetic energy E and impact parameter b . An IEM description is used for the many-electron problem. The N -electron wave function is expressed as a Slater determinant $\det(\psi_1, \dots, \psi_N)$ of single-particle wave functions ψ_i that are propagated according to

$$i \partial_t \psi_i(\mathbf{r}, t) = \hat{h}(t) \psi_i(\mathbf{r}, t), \quad i = 1, \dots, N \quad (1)$$

with a single-particle Hamiltonian of the form

$$\hat{h}(t) = -\frac{1}{2} \Delta_r + v_{\text{eff}}^t(\mathbf{r}, t) + v_{\text{eff}}^p(\mathbf{r}, t). \quad (2)$$

The total effective potential $v_{\text{eff}}^t + v_{\text{eff}}^p$ is the same for all ψ_i , and we therefore refer to it as a common potential. Both parts v_{eff}^t and v_{eff}^p consist of nuclear potentials and mean-field potentials modeling electron-electron interactions. We introduce the mean-field potentials in a no-response approximation first, followed by a brief description of the target response model used in this work.

A. No-response approximation

In the no-response approximation the effective target and projectile potentials in the Hamiltonian (2) are frozen to atomic and ionic ground-state potentials, respectively. Let r_t and r_p denote the distances of a given electron to the target and projectile nuclei, while \mathbf{r} is the electron's position vector with respect to the center of mass of both nuclei. Separated into

nuclear and electronic mean-field contributions the potentials are expressed as

$$v_{\text{eff}}^t(\mathbf{r}, t) \approx v_{\text{eff}}^t(r_t) = -\frac{Z_t}{r_t} + v_{\text{Ha}}^t(r_t) + v_x^t(r_t), \quad (3)$$

$$v_{\text{eff}}^p(\mathbf{r}, t) \approx v_{\text{eff}}^p(r_p) = -\frac{Z_p}{r_p} + v_{\text{Ha}}^p(r_p), \quad (4)$$

where Z_t and Z_p denote the charge numbers of the nuclei. In both expressions $v_{\text{Ha}}^t(r_t)$ and $v_{\text{Ha}}^p(r_p)$ are Hartree potentials of the form

$$v_{\text{Ha}}(r) = \int d^3r' \sum_i \frac{|\psi_i(t_0, \mathbf{r}')|^2}{|\mathbf{r} - \mathbf{r}'|}, \quad (5)$$

where the $\psi_i(t_0)$ are the N_t and N_p initially occupied target and projectile orbitals respectively (doubly counted if occupied by a spin-up and a spin-down electron). They are obtained from exchange-only optimized potential method (OPM) calculations [31], i.e., from self-consistent DFT structure calculations in which exact exchange is taken into account. In the case of the target atom, the OPM exchange potential v_x^t , which corrects for self-interaction contributions in v_{Ha}^t is also included in v_{eff}^t , but in the case of the projectile it is not.

This choice is informed by our main interest in this work, namely ionization of and transfer from the target. Accordingly, our v_{eff}^t is the correct no-response potential for (each) one of the N_t initial target electrons, while v_{eff}^p is the potential experienced by an electron that does not contribute to the projectile charge distribution; i.e., it is the correct potential experienced by a (distant) target electron. Note that v_{eff}^t is asymptotic to $-1/r_t$, whereas v_{eff}^p is asymptotic to $-q_p/r_p$ (q_p being the projectile charge state).

Inevitably, there is a price to pay for working with a common mean-field potential of the type $v_{\text{eff}}^t + v_{\text{eff}}^p$ if the potential is chosen such that it has the correct asymptotic behavior for an initial target electron: One cannot expect to obtain accurate results for projectile-electron transitions, since from the perspective of an initial projectile electron v_{eff}^t is too attractive while v_{eff}^p is too weak. Chiefly this leads to increased loss from the projectile, which is further discussed in Sec. III B. While a coupled mean-field approach in which electrons of both centers are propagated with different potentials that show the correct asymptotic behavior is possible, it would require us to renormalize the many-electron wave function [14], since the orthogonality of the propagated orbitals is lost. The advantage of using a common potential is that orthogonality is preserved, which makes the final-state analysis straightforward.

B. Target response

In the no-response approximation the effective potentials v_{eff}^t and v_{eff}^p are constant in time in reference systems moving with the respective centers. This should be adequate for fast collisions, in which the electrons do not have enough time to adapt to changes in the potentials. However, below a few hundred keV per nucleon a description that includes response is desirable [32]. We do so, adapting the target response model of Ref. [32] which is briefly summarized in the following: A time-dependent effective potential $v_{\text{eff}}^t(t)$ is formed as a linear combination of ionic ground-state potentials v_{q_t} weighted by

probabilities for reaching the corresponding charge states q_i . The ionic potentials are approximated by scaling the effective potential $v_{\text{eff}}^t(t_0)$ of the neutral atom such that the ionic ground-state potentials v_{q_i} show the $-1/r_t$ tail of the neutral target case for $q_t = 0$ and $q_t = 1$ while they behave like $-q_t/r_t$ for $q_t > 1$. This choice ensures that dynamical screening does not set in when only a small fraction of the electronic charge has been removed.

With this approach Ref. [32] developed the following expression for a time-dependent screening factor:

$$\alpha(t) = \frac{P_{\text{net}}^t(t) - (P_{\text{net}}^t(t)/N_t)^{N_t}}{N_t - 1}, \quad (6)$$

where $P_{\text{net}}^t(t)$ is the net occupation of bound target states¹ and $(P_{\text{net}}^t(t)/N_t)^{N_t}$ is interpreted as the probability to find all N_t electrons at the target at time t . By applying Eq. (6) in Eq. (2) we approximate the effective target potential as

$$v_{\text{eff}}^t(\mathbf{r}, t) \approx v_{\text{eff}}^t(r_t, t) = -\frac{Z_t}{r_t} + \alpha(t)[v_{\text{Ha}}^t(r_t) + v_x^t(r_t)], \quad (7)$$

with the same Hartree and exchange potentials that are used in the no-response approximation [cf. Eq. (3)]. When the net occupation equals the number of electrons of the neutral target atom, $P_{\text{net}}^t = N_t$, i.e., before the collision in particular, the time-dependent screening potential is equal to the static one, $v_{\text{eff}}^t(r_t, t) = v_{\text{eff}}^t(r_t)$.

If the single-particle wave functions $\psi_i(\mathbf{r}, t)$ are represented in a finite basis the net occupation can be calculated according to

$$P_{\text{net}}^t = \sum_{i=1}^N \sum_{\nu=1}^{V_t} |c_{\nu}^i(t)|^2 \quad (8)$$

with transition amplitudes

$$c_{\nu}^i(t) = \langle \varphi_{\nu} | \psi_i(t) \rangle \quad (9)$$

and the sum over ν includes all bound target states $|\varphi_{\nu}\rangle$ that are noticeably populated.

In Ref. [32] instantaneous target eigenstates $|\varphi_{\nu}(t)\rangle$ for the time-dependent effective target potential of Eq. (7)

$$\left(-\frac{1}{2}\Delta_{\mathbf{r}} + v_{\text{eff}}^t(t)\right)|\varphi_{\nu}(t)\rangle = \varepsilon_{\nu}(t)|\varphi_{\nu}(t)\rangle \quad (10)$$

were used in Eq. (9). In the present work we project the solutions on undisturbed target eigenstates $|\varphi_{\nu}^0\rangle = |\varphi_{\nu}(t_0)\rangle$ instead. It has been shown in Ref. [32] that projecting on instantaneous states is preferable, because it avoids oscillations of the target net occupation P_{net}^t which arise in an analysis based on the undisturbed target states $|\varphi_{\nu}^0\rangle$ due to a lack of synchronization with the time-dependent potential.

We make this seemingly unfavorable choice in the present work for the following reasons. As explained in Sec. II C we use the TC-BGM to represent the IEM collision problem. A TC-BGM basis consists of bound target, bound projectile, and BGM pseudostates. In Ref. [32] a BGM basis without

projectile states was used instead. This made the extraction of electron transfer amplitudes more difficult, but it was straightforward to obtain the instantaneous states of Eq. (10) by diagonalization. This is different in the present case of a (nonorthogonal) two-center basis, in which the definition of the target net occupation becomes somewhat arbitrary when target and projectile states overlap at small internuclear distances. Regarding the asymptotic instability of P_{net}^t it was demonstrated in Ref. [32] that an averaging procedure involving results in a certain interval of large projectile-target distances gave very similar results as the analysis in terms of the instantaneous eigenstates (10). Auxiliary calculations (not shown) indicate that this is also the case for the collision systems studied here—with some limitations at high projectile energy as discussed further below in Sec. III A.

Transition probabilities for initial conditions at the projectile are part of the sum in Eq. (8). As a consequence, the target net occupation can exceed the number of electrons of the neutral atom, $P_{\text{net}}^t > N_t$. When this happens, P_{net}^t/N_t exceeds unity and loses its probabilistic interpretation. This was of no concern in Ref. [32] since the calculations did not consider active electrons of the projectile. We remedy this in the present work by capping the target net occupation P_{net}^t at N_t . In practice, we found it rarely happens that the target net occupation P_{net}^t exceeds $N_t = 10$ (for neon), and if it does, it is only by a small margin (≈ 0.1). Hence, we deem the simple procedure of capping P_{net}^t to be unproblematic.

C. Basis generator method

The single-particle equations (1) are solved using a finite basis expansion obtained from the TC-BGM [29]. A TC-BGM basis $\{|\chi_{\nu}^{\mu}\rangle\}$ consists of sets of atomic target states $\{|\varphi_{\nu}^0\rangle, \nu = 1, \dots, V_t\}$, ionic eigenstates of the projectile $\{|\varphi_{\nu}^0\rangle, \nu = V_t + 1, \dots, V\}$, and pseudostates. The latter are dynamically generated from the target atomic orbitals by application of powers of a regularized projectile potential operator $W_p = (1 - e^{-r_p})/r_p$. Reference [16] established that for the finite vector space spanned by such a basis the coupling to the complementary part of Hilbert space is minimal. The construction rule for the basis is

$$|\chi_{\nu}^{\mu}(t)\rangle = [W_p(t)]^{\mu} |\varphi_{\nu}^0\rangle \quad \mu = 0, \dots, M_{\nu}, \quad (11)$$

TABLE I. Maximum power M_{ν} of the potential operator in Eq. (11) for all ν corresponding to target subshells 2s to 4f; each set of M_{ν} defines the construction of a basis of size N_{χ} . The basis for $N_{\chi} = 185$, marked with boldface in the table, was used to calculate the results of Sec. III.

M_{ν} for orbitals									
2s	2p	3s	3p	3d	4s	4p	4d	4f	N_{χ}
0	1	2	2	4	5	5	5	5	170
0	1	2	2	4	5	5	5	6	177
0	1	2	3	4	5	5	5	6	180
0	1	2	3	4	5	5	6	6	185
0	1	2	3	4	6	6	6	6	189

¹In Ref. [32] the scaling is written as function of the target net removal $P_{\text{net}}^{\text{loss}}$, while the net occupation $P_{\text{net}}^t = N_t - P_{\text{net}}^{\text{loss}}$ is used here.

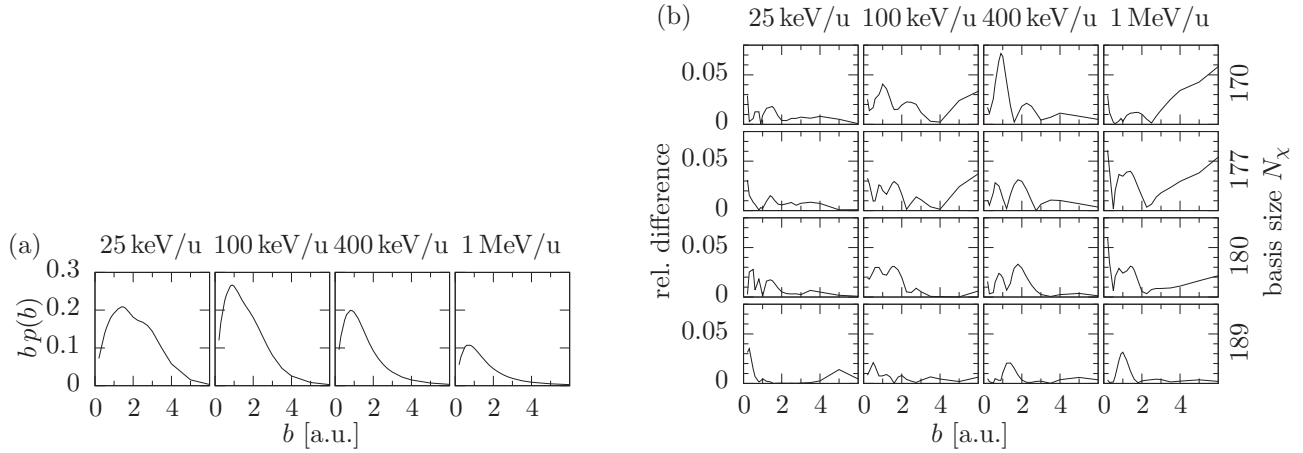


FIG. 1. (a) Weighted average probabilities $b \bar{p}^m(b)$ for target electron removal, calculated with a basis spanned by $N_\chi = 185$ states. (b) Relative difference $|\bar{p}_{N_\chi}^m / \bar{p}_{185}^m - 1|$ of the above basis to bases comprising 170, 177, 180, and 189 states (cf. Table I).

where $M_\nu = 0$ for $\nu > V_t$. Table I lists several examples for M_ν , jointly denoting the values for all ν of the same subshell. A set of M_ν corresponds to N_χ basis states. It is chosen such that sufficient convergence with regard to the observables of interest is achieved. Figure 1(a) shows the average of the B^{2+} -Ne target electron removal probability $\bar{p}^m = (N_t - P_{\text{net}}^t) / N_t$ as a function of, and weighted by, the impact parameter b for the basis consisting of 185 states (cf. Table I). The relative differences $|\bar{p}_{N_\chi} / \bar{p}_{185} - 1|$ to probabilities calculated with three smaller bases ($N_\chi = 170, 177$, and 180) and one larger basis ($N_\chi = 189$) are shown in Fig. 1(b). With the exception of the smallest basis (170 states) the differences to the $N_\chi = 185$ basis are well below 5%. The $N_\chi = 185$ basis is used for all further calculations in this work. Basis convergence for the other collision systems is comparable.

The $1s$ target state is not included in the TC-BGM basis, since these electrons are tightly bound and can be considered as a frozen core in the impact energy range of interest. We have verified this assumption for the B^{2+} -Ne collision system.

In addition to the $(2s-4f)$ target states and the BGM pseudostates we include 20 ionic eigenstates, $1s, \dots, 4f$, for all four projectiles in our basis. In the case of the bare ions, He^{2+} and Li^{3+} , analytical hydrogenlike functions are used. Numerical solutions of the Schrödinger equation for the effective potentials $v_{\text{eff}}^p(r)$ are used for the dressed projectiles B^{2+} and C^{3+} .

D. Final-state analysis

The immediate results of the dynamic calculations are the transition amplitudes c_n^i at $t = t_f$ [cf. Eq. (9)]. An observable that can be compared with experiments and that is found quite directly from a number of calculations covering a range of impact parameters b is the net recoil ion production cross section σ_+ . It can be expressed via the target net occupation P_{net}^t [cf. Eq. (8)]:

$$\sigma_+ = 2\pi \int_0^\infty b [N_t - P_{\text{net}}^t(b)] db. \quad (12)$$

Additional considerations are required to move from the single-particle view to many-particle observables. A first

step is to define an exclusive probability $P_{\varphi_1, \dots, \varphi_N}$ to find the system in a specific final configuration, an N -electron state $|\varphi_1, \dots, \varphi_N\rangle$ represented by a Slater determinant composed from $\varphi_n \in \{\varphi_\nu^0, \nu = 1, \dots, V\}$. The collision system at final time t_f is described by the state $|\psi_1, \dots, \psi_N\rangle$ that is formed from propagated single-particle wave functions ψ_i [cf. Eq. (1)]. The exclusive probability

$$P_{\varphi_1, \dots, \varphi_N} = |\langle \psi_1, \dots, \psi_N | \varphi_1, \dots, \varphi_N \rangle|^2 \quad (13)$$

can be expressed as the determinant of the $N \times N$ density matrix γ with matrix elements

$$\gamma_{nn'} = \sum_{i=1}^N \langle \varphi_n | \psi_i \rangle \langle \psi_i | \varphi_{n'} \rangle = \sum_{i=1}^N c_n^i c_{n'}^{i*} \quad \text{at } t = t_f, \quad (14)$$

where the c_n^i are those transition amplitudes of Eq. (9) that correspond to the final configuration considered.

While it is possible to evaluate all observables of interest by combinations of exclusive probabilities, it requires great computational effort. We avoid this through the inclusive probability approach of Ref. [33]. Selecting and evaluating a smaller $m \times m$ determinant of the density matrix yields an inclusive probability to find m specific states occupied by electrons, while the final states of the remaining $N - m$ electrons are not determined [33]. Through combinations of inclusive probabilities one can obtain probabilities p_{kl} for a final configuration where k electrons are at the projectile, l in the continuum, and $N - k - l$ at the target [34]. The total cross section corresponding to such a charge-state correlated measurement is

$$\sigma_{kl} = 2\pi \int_0^\infty b p_{kl}(b) db. \quad (15)$$

Summation of all σ_{kl} weighted with the final target charge state $q_t^f = k + l - N_p$ yields an expression equivalent to Eq. (12) for the net recoil ion production:

$$\sigma_+ = \sum_{k=0}^N \sum_{l=0}^{N-k} (k + l - N_p) \sigma_{kl}. \quad (16)$$

For the results presented below transition amplitudes to target $n = 4$ states are not considered in the determinantal final-state analysis, although they are included in the TC-BGM basis, in order to reduce computational complexity. We verified on the level of single-particle probabilities that transitions to these states are negligible.

III. RESULTS

A. Response vs no-response calculations

In Ref. [32] target response in BGM calculations for He^{2+} -Ne collisions was investigated. In this work we apply the same response model to collisions of neon atoms with dressed ions. We begin the discussion with comparing the present results for the B^{2+} -Ne system to a previous no-response calculation [28]. Both sets of calculations consider active target and projectile electrons, labeled BGM-TP in Ref. [28]. They differ only with regard to modeling response and the effects thereof.

Total cross sections σ_{3l} for pure multiple ionization, coincident with an unchanged projectile charge state $q_p^i = q_p^f$, are shown in Fig. 2. Experimental results from Ref. [20] are included as well. For single-ionization σ_{31} response and no-response calculations provide nearly coinciding curves. This similarity is a consequence of the soft onset of the screening model of Eqs. (6) and (7), where a small reduction of target net occupation P_{net}^i weakens the screening potential only marginally.

As the number of electrons in the continuum l increases, the calculations become more distinct. For σ_{33} response underestimates the experiment below the velocity $v = 3$ a.u., while the no-response calculation is in good agreement with

the data. In the case of fourfold ionization σ_{34} the no-response calculation overestimates the experiment while response underestimates it for $v < 3$ a.u.. This indicates that response has the tendency to weaken multiple ionization, which becomes most evident for fivefold ionization σ_{35} . The no-response calculation overestimates the experiment considerably, while response overestimates the experiment to a lesser degree.

We have argued in Sec. II B that the no-response approximation is adequate for the description of fast collisions. In this context the discrepancy between the two calculations above $v = 5$ a.u., in particular visible when several electrons are removed, suggests a failure of the response calculation. A detailed analysis has shown that use of undisturbed $|\varphi_v^0\rangle$ rather than instantaneous $|\varphi_v(t)\rangle$ atomic target eigenstates for determining the target net occupation P_{net}^i and for carrying out the final-state analysis is responsible for the discrepancies (cf. Sec. II B). For slower collisions the effect of using the undisturbed states cannot be evaluated by comparing the response and no-response calculations. However, a comparison of present He^{2+} -Ne results with those of Ref. [32], for which the same response model with instantaneous target states was used, does not show a noticeable discrepancy in this energy range. That is, the problems of the response calculations seem to be restricted to high energies. They are somewhat reminiscent of the shake-off mechanism, in which the sudden removal of one electron causes multiple ionization due to nonzero overlaps of undisturbed target states with the continuum of the ion. However, we deem them to be unphysical in the present context of an IEM calculation with a suddenly changing effective potential.

We have found that the role of target response is most pronounced in target ionization channels. Of the capture channels of interest here, single and double capture, the former is unaffected and the latter has its cross sections only slightly lowered by response.

Collisions with the triply charged projectiles C^{3+} and Li^{3+} show the same patterns regarding the comparison of no-response and response calculations, albeit on a smaller scale.

B. Doubly charged projectiles

In the following only target response calculations are considered. They agree better with experimental data for He^{2+} projectiles than their no-response counterparts, as shown in Ref. [32], while, as discussed above, in the case of B^{2+} the response effect is small.

Figure 3 compares the weighted sum of the pure target ionization cross sections, which we refer to as pure ion production in the following²

$$\sigma_+^{\text{pure}} = \sum_{l=1}^{N-k} l \sigma_{kl} \quad \text{for } k = Z_p - q_p^i, \quad (17)$$

²In our previous works [28,30], we called this quantity positive ion production and used the symbol $\tilde{\sigma}_+$. In this article, the name was changed to pure ion production σ_+^{pure} in order to avoid confusion with the net recoil ion production σ_+ .

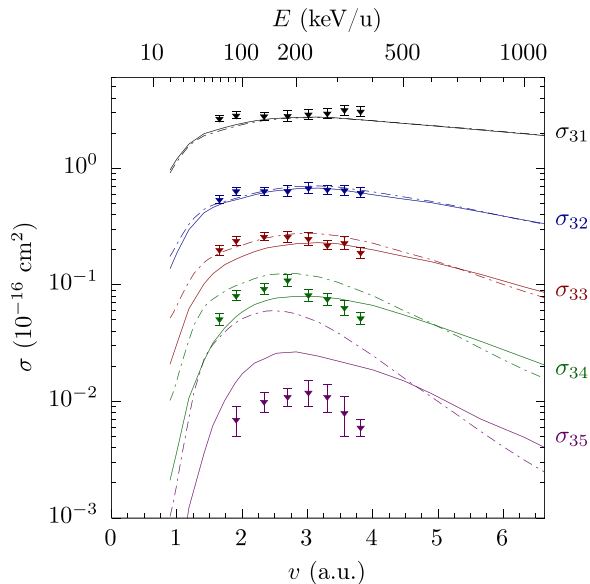


FIG. 2. (Color online) Total cross sections for projectile-charge-state-coincident multiple ionization of Ne by B^{2+} as functions of projectile velocity v , comparing response (solid lines) and no-response [28] (dash-dotted lines) calculations. Shown are four groups (set apart by color) for final target charge states $q_t^f = 1, \dots, 5$. The projectile charge state is fixed at $q_p^i = q_p^f = 2$. Experimental data are from Ref. [20].

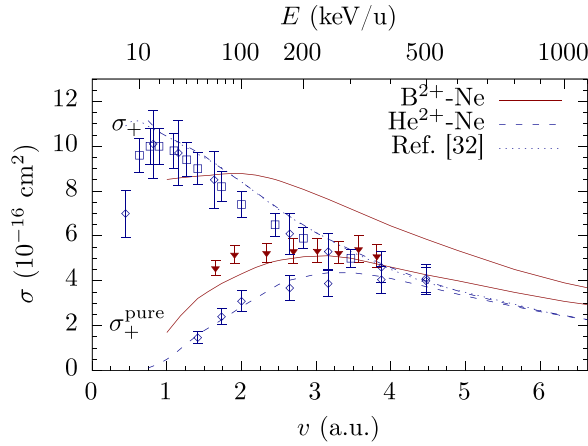


FIG. 3. (Color online) Net recoil ion production σ_+ and pure ion production σ_+^{pure} for Ne by B^{2+} (solid line), He^{2+} ion impact from present (long-dashed line) and Ref. [32] (short-dashed line) calculations. What appears to be a dash-dotted line are in fact the two He^{2+} -Ne σ_+ lines in close proximity. Experimental data: B^{2+} [20] (filled triangles), He^{2+} [35] (open squares), and [36] (open lozenges).

for the two $q_p^i = 2$ collision systems He^{2+} -Ne and B^{2+} -Ne. To stay consistent with the experiments of Ref. [36], the figure shows the truncated sum ($l \leq 4$) for σ_+^{pure} rather than the full sum.

For He^{2+} the present theory is in very good agreement with the measurements [35,36] over the whole measured range. Likewise, σ_+^{pure} is mostly in good agreement with the experiment for B^{2+} [20]. For relatively slow collisions ($v < 2.5$ a.u.) the experimental data points are somewhat underestimated, however. Pure ion production by the dressed boron ion is enhanced in comparison to that by the bare helium ion. At high energies this can be explained straightforwardly. In this regime multiple ionization occurs predominantly in close collisions ($b < 1$ a.u.) for which the B^{2+} potential becomes

stronger than that of He^{2+} around the closest approach as a consequence of an incomplete screening of the nucleus.

The resulting increase of multiple ionization is partially compensated by coincident loss of projectile electrons, reducing the probability of a pure-ionization final state. This can be seen when comparing the σ_+^{pure} curve with the net recoil ion production σ_+ [cf. Eqs. (12) and (16)] also displayed in Fig. 3. This cross section also includes collision channels with a final projectile charge state different from the initial one. While the bare helium σ_+^{pure} and σ_+ curves converge, as capture becomes less likely with increasing relative velocity, a gap remains for B^{2+} .

In slow collisions the capture probabilities exceed those of ionization. While direct ionization is still present at the lowest collision energies considered in this work, pure ionization channels are considerably smaller than channels involving electron capture. This is in particular the case for the helium projectile, where pure ion production is an order of magnitude smaller than net recoil ion production. Note that the agreement between theoretical and experimental σ_+ results is good for He^{2+} projectiles except at the lowest impact energy. Unfortunately, no experimental σ_+ data are available for the B^{2+} case.

The gap between the pure ion production by the two projectiles is wider at low and intermediate velocities $v < 3$ a.u. than at high velocities. This can be explained with stronger capture by the helium ion. Also of importance are transfer-ionization processes in which the initial projectile electrons are involved. For example, consider a process where one electron is captured by the projectile while an initial projectile electron is lost to the continuum, resulting in an unchanged projectile charge state and contributing to σ_+^{pure} . In other words, in bare ion collisions capture removes probability from the pure ionization channels, whereas in the case of dressed ions this can be somewhat compensated by transfer-ionization processes like the one described above. In

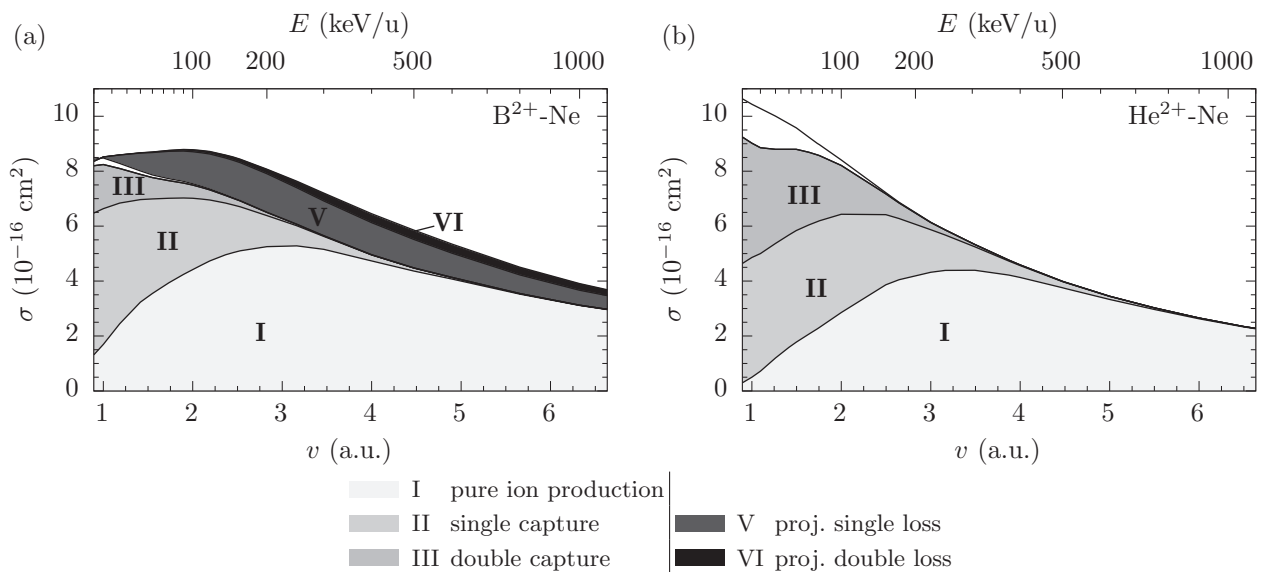


FIG. 4. Contributions to the net recoil ion production σ_+ grouped by the final projectile charge state q_p^f that the weighted multiple ionization terms in Eq. (18) are coincident with. The topmost curves are identical to the respective σ_+ curves in Fig. 3. (a) B^{2+} -Ne collisions, and (b) He^{2+} -Ne collisions.

a previous work [28] we found indications that such processes are indeed significant in this energy range. The larger number of possible processes for a dressed projectile leading to the same final electron configuration might also be a reason for the observation that the B^{2+} calculation does not agree as well with the experimental data as the He^{2+} calculation.

The large gap between σ_+ and σ_+^{pure} in slow collisions due to capture and transfer ionization prompts a closer look at these contributions. Let us focus on the B^{2+} case and rewrite Eq. (16) as

$$\sigma_+ = \underbrace{\sigma_+^{\text{pure}}}_{\text{I}} + \underbrace{\sum_{l=0}^7 (l+1)\sigma_{4l}}_{\text{II}} + \underbrace{\sum_{l=0}^6 (l+2)\sigma_{5l}}_{\text{III}} + \dots + \underbrace{\sum_{l=1}^9 (l-1)\sigma_{2l}}_{\text{V}} + \underbrace{\sum_{l=2}^{10} (l-2)\sigma_{1l}}_{\text{VI}} + \dots \quad (18)$$

In Fig. 4 the terms denoted by Roman numerals are consecutively added. The terms are labeled correspondingly for He^{2+} impact, bearing the different q_p^i in mind. In slow B^{2+} -Ne collisions, single capture and transfer ionization (II) processes give the largest contribution, greatly exceeding processes where two electrons are captured (III).

The empty area between the areas denoted III and V represents capture processes where the number of electrons at the projectile k exceeds its nuclear charge number Z_p , corresponding to negative ion production. These unphysical contributions are a consequence of the statistical treatment of multiple electron processes used in the IEM. While it is significant in the case of He^{2+} impact [Fig. 4(b)], the net recoil ion production is unaffected by the deficiencies of the statistical model as it can be directly calculated from single-particle probabilities [cf. Eqs. (8) and (12)].

Projectile electron loss (V) sets in at the lowest impact energies considered, increases with increasing E , and remains fairly constant for $E \geq 100$ keV/u. Double-projectile electron loss is noticeable but not significant over the investigated energy range. Triple projectile loss is negligible. For low

impact energies, projectile electron loss probabilities are overestimated due to our choice of potentials in Eq. (2). Moreover, our description does not include antiscreening [37], which greatly enhances ionization of the projectile in fast collisions. Based on a comparison with projectile electron loss experiments [22] we expect an uncertainty of at least a factor of two for these channels.

When comparing He^{2+} with B^{2+} impact [Fig. 4(b) vs Fig. 4(a)], a notable difference is an increase of double capture (area III) by the bare ion, matching the contribution of single capture for the slowest collisions. This explains what is seen in Fig. 3: The He^{2+} -Ne σ_+ curve intersects at about $v = 2$ a.u. with that for B^{2+} and exceeds it considerably. Note that this feature does not occur in the $q_p^i = 3$ collision systems discussed below.

Including all collision channels where $q_p^f = q_p^i - 1$ the total cross section for single capture

$$\sigma_{sc} = \sum_{l=0}^{N-k} \sigma_{kl} \quad \text{for } k = Z_p - q_p^i + 1 \quad (19)$$

is shown in Fig. 5(a). The double-capture cross section σ_{dc} is similar to Eq. (19), for $k = Z_p - q_p^i + 2$, and can be found in Fig. 5(b).

Our B^{2+} -Ne results considerably underestimate the experimental total single-capture cross sections of Ref. [22] and overestimate two data points from Ref. [38]. The present theory is in good agreement with He^{2+} -Ne experiments from Ref. [36], while it overestimates the data of Ref. [35]. Comparing B^{2+} and He^{2+} impact, we find that single capture by the latter exceeds the former for all but the slowest collisions investigated.

The agreement between our results for double capture by the boron ion and the experiment of Ref. [22] is good; the data points of Ref. [38] are overestimated, however. In the case of the helium projectile, the data points of Refs. [36] and [35] are in close proximity to each other, and our calculations overestimate both. Since dynamic and final-state correlations often play an important role in double capture [39], the IEM tends to overestimate this channel. With this in mind, we consider the good agreement with the experiment

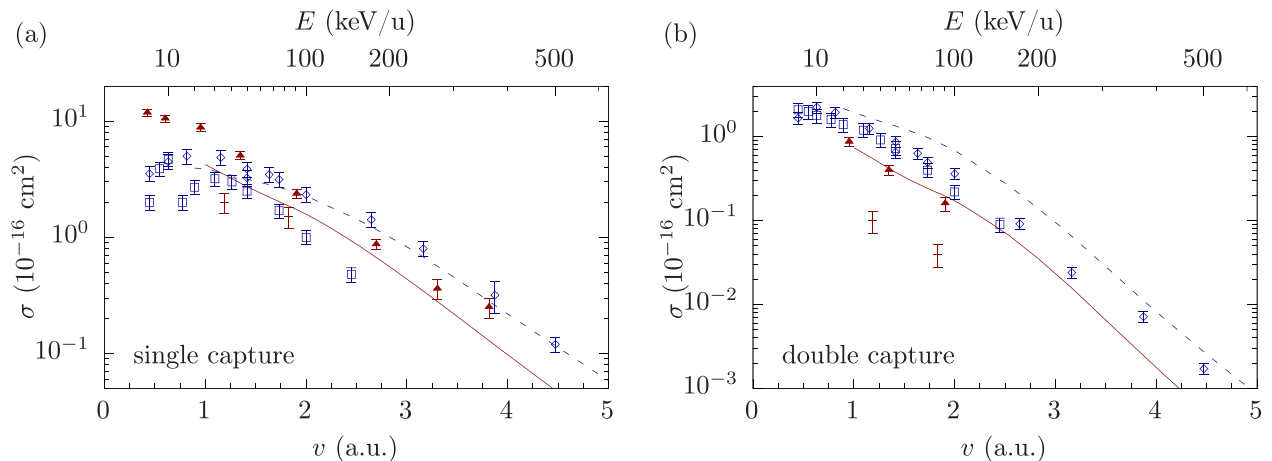


FIG. 5. (Color online) Total cross sections for (a) single- and (b) double-electron capture by B^{2+} (solid lines) and He^{2+} (dashed lines) impact on neon targets. Experimental data: B^{2+} [38] (stars), [22] (filled triangles); and He^{2+} [35] (open squares), [36] (open lozenges).

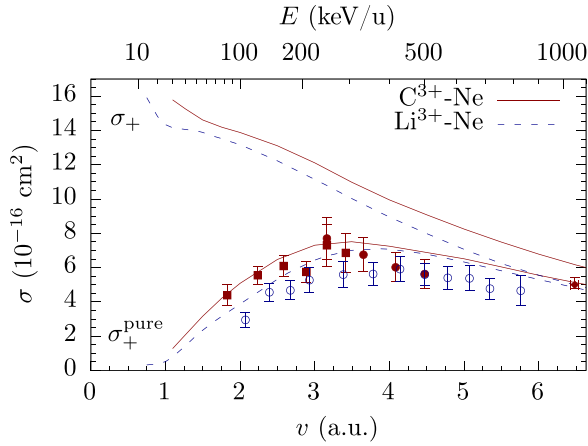


FIG. 6. (Color online) Net recoil ion production σ_+ and pure ion production σ_+^{pure} for Ne by C^{3+} (solid line) and Li^{3+} (dashed line) ion impact. Experimental data: Li^{3+} [26] (open circles); and C^{3+} [15] (filled squares), [26] (filled circles). The C^{3+} -Ne data point at $v = 6.5$ a.u. is from Ref. [40].

of Ref. [22] to be fortuitous. Moreover, if the boron curve were lower by the same factor by which the helium curve overestimates the experiments, it would lie between both sets of experimental data (viz. Refs. [22] and [38]). While this channel is overestimated, it is overestimated consistently for both projectile ions, and we can discuss them in relation to each other: Over the whole impact energy range, double capture into the bare helium ion exceeds that into the dressed boron ion, reflecting what is also apparent from the experiments.

When considering the contribution of capture to net recoil ion production, as discussed for Fig. 4, two caveats have to be kept in mind: The total cross sections σ_{sc} and σ_{dc} include all final target charge states [cf. Eq. (19)]. Since there is no weighting with the target charge state q_i^f , they cannot be identified with terms II and III in Eq. (18). However, our

findings for σ_{sc} and σ_{dc} do reflect the strong contribution of single and double capture to net recoil ion production in the He^{2+} -Ne collision system, and in turn provide an explanation for the net recoil ion production by the helium ion exceeding that of the boron ion. The caveats are somewhat alleviated as the σ_{kl} of our calculations show that for the impact energy range of most interest for this question, capture without ionization ($l = 0$) outweighs transfer ionization processes ($l \geq 1$). Cross sections for the latter measure up to the former only from $v \approx 3$ a.u. on.

C. Triply charged projectiles

Figure 6 shows the pure ion production σ_+^{pure} and the net recoil ion production σ_+ for the triply charged projectile ions C^{3+} and Li^{3+} . Our σ_+^{pure} results are mostly in good agreement with experimental data for C^{3+} [15,26,40]. The apparent structure in the experimental data around $v = 3$ a.u. is not explained by our model. Above $v \geq 4$ a.u. our calculations overestimate the results of Ref. [26], but they agree very well with the single datum of Ref. [40] at 1050 keV/u. Our results also overestimate the Li^{3+} experiments from Ref. [26]. However, in the same manner as the experimental data do, the calculated pure ion production cross sections for C^{3+} projectiles exceed those for Li^{3+} in slow collisions, while both curves converge with increasing velocity.

The calculated net recoil ion production for collisions with the carbon ion is larger than that for the lithium ion over the whole investigated impact velocity range. This is in contrast to our findings for the $q_p^i = 2$ collision systems (Fig. 3) where the bare- and dressed-ion curves intersect at $v = 2$ a.u. The σ_+ and σ_+^{pure} curves for the bare lithium ion converge as the impact energy increases, while those for the dressed carbon ion stay apart. Similarly to the B^{2+} -Ne case, this can be attributed to projectile electron loss, as is apparent from the areas denoted as V and VI in Fig. 7(a). The designations in this figure follow

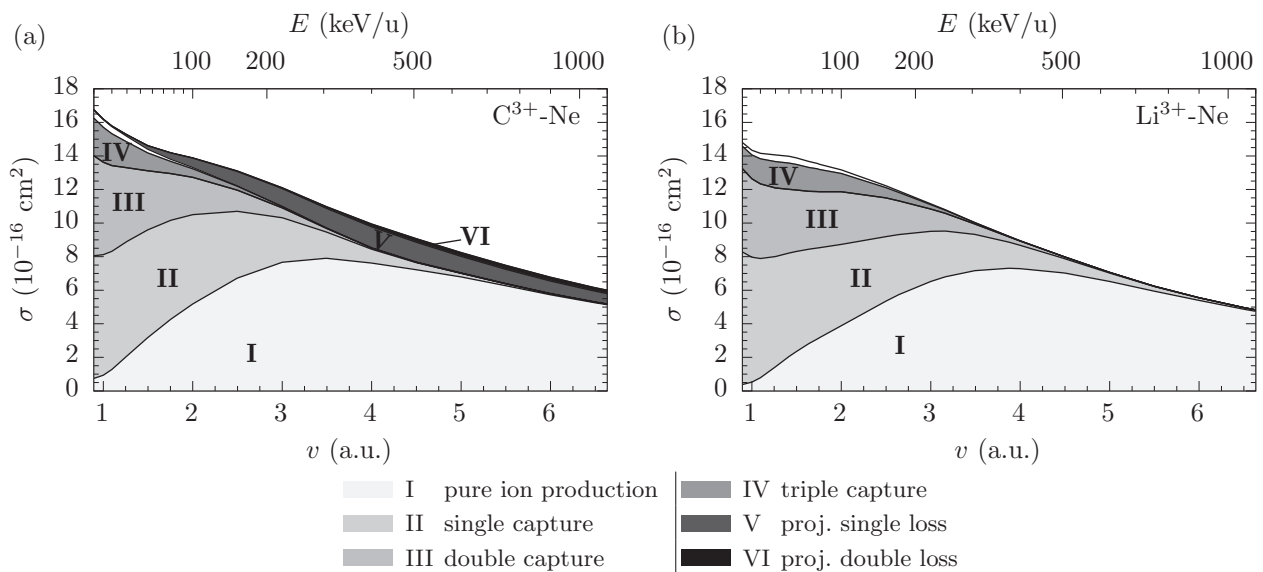


FIG. 7. Contributions to the net recoil ion production σ_+ grouped by the final projectile charge state q_p^f the weighted multiple ionization terms in Eq. (18) are coincident with. The topmost curves are identical to the respective σ_+ curves in Fig. 6. (a) C^{3+} -Ne collisions, and (b) Li^{3+} -Ne collisions.

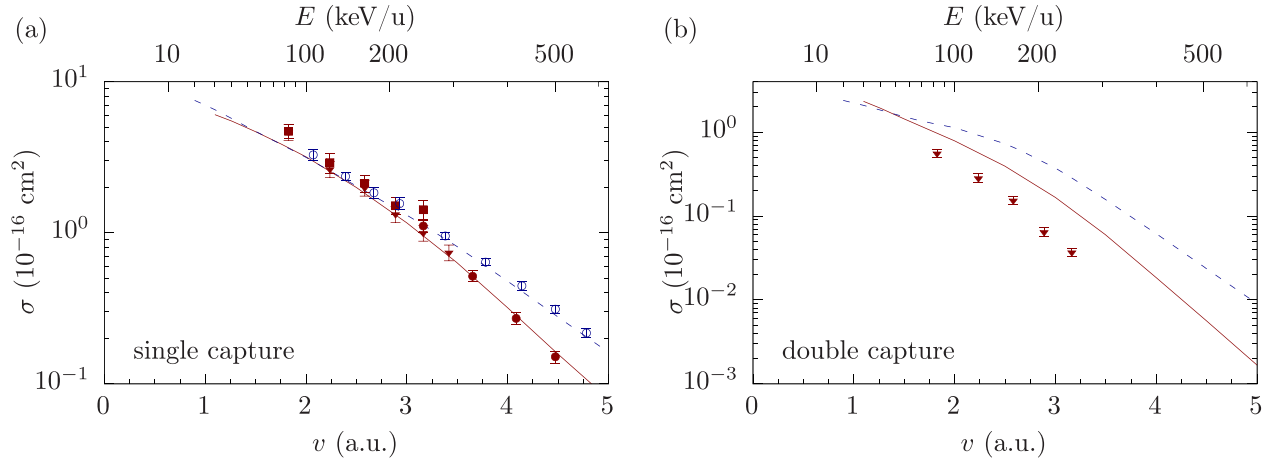


FIG. 8. (Color online) Total cross sections for (a) single- and (b) double-electron capture by C^{3+} (solid lines) and Li^{3+} (dashed lines) impact on neon targets. Experimental data: C^{3+} [15] (filled squares), [26] (filled circles), [21] (filled triangles); and Li^{3+} [26] (open circles).

the notation introduced in Eq. (18) plus $\sum_{l=0}^5(l+3)\sigma_{6l}$ for the contribution of triple-capture processes to σ_+ , denoted as IV. For both triply charged projectiles the contribution of capture processes becomes smaller as the number of captured electrons increases, which is different from He^{2+} impact, where the contributions from double capture can exceed those from single capture. Also unlike He^{2+} -Ne, for Li^{3+} -Ne collisions the contributions from capture processes with $k > Z_p$ are not significant as can be inferred from the negligibly small white areas in Fig. 7(b).

Our calculations for C^{3+} and Li^{3+} single-capture cross sections σ_{sc} [cf. Eq. (19)] are in good overall agreement with experiments shown in Fig. 8(a) with two data points for C^{3+} at 83 keV/u being somewhat underestimated.³ We find single capture into the bare lithium ion slightly enhanced in comparison to the dressed carbon ion. Our calculation overestimates experimental C^{3+} double capture σ_{dc} [Fig. 8(b)]. Similar to the collisions with doubly charged projectiles, this is due to the IEM's inability to describe correlated capture processes. Calculated double-capture cross sections for the lithium ion exceed those for the carbon ion at mid- to high energies, while the curves intersect at about $E = 50$ keV/u. We are not aware of experimental σ_{dc} for Li^{3+} impact.

IV. CONCLUSIONS

We presented TC-BGM calculations for collisions of bare and dressed ions with neon atoms, using an IEM description. In the dressed-ion case orbitals of both collision centers were propagated in a common mean field. Resulting many-electron wave functions were expressed as single Slater determinants, and transition probabilities to final states were found with the inclusive probability method, which reduces the combinatoric complexity of the problem.

Time-dependent screening of the target nucleus was addressed with a response model in which the screening potential is a function of target occupation. When both

collision centers are at close proximity, the concept of target occupation becomes a matter of definition within the IEM. We chose a pragmatic approach and projected the propagated single-particle wave functions on atomic eigenstates. Results calculated with the present response model were compared with results of the no-response approximation. It was found that total cross sections for pure single and double ionization of Ne in collisions with B^{2+} hardly differ in both calculations. The effect of response, suppressing multiple ionization due to reduced screening, becomes more apparent as the number of removed electrons increases. In the case of threefold ionization, this led to an underestimation of the experimental data, while the no-response results are in excellent agreement. At this point it cannot be established if this has to be attributed to the simplicity of the global response model or if it points to a more fundamental limitation of the IEM for processes that involve three or more electrons. Experience from previous calculations, e.g., Refs. [13,32,41,42], suggests a tendency of the IEM to overestimate multiple ionization when the final target charge state exceeds the initial projectile charge state by more than one [28]. While the no-response as well as the response results are in reasonable agreement with the experiment, we favor the response calculations for systematic reasons.

Accordingly, all further calculations for B^{2+} and C^{3+} impact on Ne were carried out using the present response model. To serve as a reference, collisions with He^{2+} and Li^{3+} projectiles were calculated with a consistent set of parameters. For all collision systems our results for net recoil ion production and pure ion production agree nicely with the available experimental data. Results for single capture are mostly in reasonable agreement with experiments, but double capture is overestimated, as is typically the case in IEM descriptions.

We found net recoil ion production by bare-ion impact to exceed that by dressed ions when comparing He^{2+} and B^{2+} impact. This is usually not expected in comparisons of bare- and dressed-ion collisions and was not found when comparing impacts by Li^{3+} and C^{3+} ions. By breaking the net recoil ion production down into its contributing cross sections, each corresponding to a final projectile charge state, it is found that capture into the projectile is responsible for the increase of net

³The σ_{sc} from Ref. [15] is the sum of the transfer ionization channels $\sum_{l=0}^3 \sigma_{4l}$, corresponding to final neon charge states 1 to 4.

recoil ion production by He^{2+} impact. In other words, net recoil ion production by He^{2+} impact is increased because capture into He^{2+} is stronger than into B^{2+} .

We consider the results of the present model to be in good overall agreement with the experimental data, and find it remarkable that a large number of collision channels corresponding to quite different processes are resulting from one calculation. A complete picture, also including projectile loss channels, is hindered by the limitation of having the exchange potential localized at one center, leading to wrong asymptotic potentials for electrons at the other. Such limitations of the IEM in the form we use it, based on the electronic density of both centers before the collision, can often be bypassed through superimposed models. The aforementioned asymptotic problem would be eluded by a piecewise potential function. The present global target response model is an example for such an approach, modeling response by scaling the screening potential with a factor depending on target occupation, and indeed could be done for the projectile as well [13]. There is,

however, the danger of overburdening the IEM or blurring the first-principles approach, due to the need for free parameters and pragmatic definitions. If a more complete picture is sought, it might be a better idea to construct a microscopic response potential [43]. Based on exchange-only DFT this is feasible and worthwhile pursuing, since such a calculation may be viewed as the exact no-correlation limit, i.e., the best possible IEM one can come up with. It is possible in principle to follow this avenue further and include correlation effects in the DFT context, but given the fundamental and practical difficulties associated with constructing a suitable correlation potential and the observables of interest [44] this will remain a challenge for some time to come.

ACKNOWLEDGMENTS

The financial support of the National Sciences and Engineering Council of Canada is gratefully acknowledged.

-
- [1] D. R. Schultz, R. E. Olson, C. O. Reinhold, S. Kelbch, C. Kelbch, H. Schmidt-Böcking, and J. Ullrich, *J. Phys. B* **23**, 3839 (1990).
 - [2] R. E. Olson and A. Salop, *Phys. Rev. A* **16**, 531 (1977).
 - [3] F. T. Chan and J. Eichler, *Phys. Rev. Lett.* **42**, 58 (1979).
 - [4] L. H. Toburen, N. Stolterfoht, P. Ziem, and D. Schneider, *Phys. Rev. A* **24**, 1741 (1981).
 - [5] J. K. M. Eichler, A. Tsuji, and T. Ishihara, *Phys. Rev. A* **23**, 2833 (1981).
 - [6] L. H. Toburen, R. D. DuBois, C. O. Reinhold, D. R. Schultz, and R. E. Olson, *Phys. Rev. A* **42**, 5338 (1990).
 - [7] M. Das, M. Purkait, and C. R. Mandal, *Phys. Rev. A* **57**, 3573 (1998).
 - [8] D. Fregenal, J. M. Monti, J. Fiol, P. D. Fainstein, R. D. Rivarola, G. Bernardi, and S. Suárez, *J. Phys. B* **47**, 155204 (2014).
 - [9] J. M. Monti, R. D. Rivarola, and P. D. Fainstein, *J. Phys. B* **41**, 201001 (2008).
 - [10] V. Rodríguez, *Nucl. Instrum. Methods Phys. Res. B* **205**, 498 (2003).
 - [11] J. M. Monti, R. D. Rivarola, and P. D. Fainstein, *J. Phys. B* **44**, 195206 (2011).
 - [12] T. Kirchner and M. Horbatsch, *Phys. Rev. A* **63**, 062718 (2001).
 - [13] T. Kirchner, M. Horbatsch, and H. J. Lüdde, *Phys. Rev. A* **64**, 012711 (2001).
 - [14] T. Kirchner, M. Horbatsch, and H. J. Lüdde, *J. Phys. B* **37**, 2379 (2004).
 - [15] T. Kirchner, A. C. F. Santos, H. Luna, M. M. Sant'Anna, W. S. Melo, G. M. Sigaud, and E. C. Montenegro, *Phys. Rev. A* **72**, 012707 (2005).
 - [16] O. J. Kroneisen, H. J. Lüdde, T. Kirchner, and R. M. Dreizler, *J. Phys. A* **32**, 2141 (1999).
 - [17] J. E. Miraglia and M. S. Gravielle, *Phys. Rev. A* **81**, 042709 (2010).
 - [18] C. C. Montanari, E. C. Montenegro, and J. E. Miraglia, *J. Phys. B* **43**, 165201 (2010).
 - [19] C. C. Montanari, J. E. Miraglia, W. Wolff, H. Luna, A. C. F. Santos, and E. C. Montenegro, *J. Phys.: Conf. Ser.* **388**, 012036 (2012).
 - [20] W. Wolff, H. Luna, A. C. F. Santos, E. C. Montenegro, R. D. DuBois, C. C. Montanari, and J. E. Miraglia, *Phys. Rev. A* **84**, 042704 (2011).
 - [21] W. S. Melo, M. M. Sant'Anna, A. C. F. Santos, G. M. Sigaud, and E. C. Montenegro, *Phys. Rev. A* **60**, 1124 (1999).
 - [22] W. Wolff, H. Luna, A. C. F. Santos, E. C. Montenegro, and G. M. Sigaud, *Phys. Rev. A* **80**, 032703 (2009).
 - [23] W. Wolff, I. J. de Souza, A. C. Tavares, G. F. S. de Oliveira, and H. Luna, *Rev. Sci. Instrum.* **83**, 123107 (2012).
 - [24] A. C. F. Santos, G. M. Sigaud, W. S. Melo, M. M. Sant'Anna, and E. C. Montenegro, *Phys. Rev. A* **82**, 012704 (2010).
 - [25] H. Luna, I. Junger, A. C. P. Cordeiro, W. Wolff, E. C. Montenegro, C. C. Montanari, and J. E. Miraglia, *J. Phys.: Conf. Ser.* **388**, 082003 (2012).
 - [26] J. S. Ihani, H. Luna, W. Wolff, and E. C. Montenegro, *J. Phys. B* **46**, 115208 (2013).
 - [27] A. L. C. Losqui, F. Zappa, G. M. Sigaud, W. Wolff, M. M. Sant'Anna, A. C. F. Santos, H. Luna, and W. S. Melo, *J. Phys. B* **47**, 045202 (2014).
 - [28] G. Schenk, M. Horbatsch, and T. Kirchner, *Phys. Rev. A* **88**, 012712 (2013).
 - [29] M. Zapukhlyak, T. Kirchner, H. J. Lüdde, S. Knoop, R. Morgenstern, and R. Hoekstra, *J. Phys. B* **38**, 2353 (2005).
 - [30] G. Schenk and T. Kirchner, *Phys. Procedia* (accepted).
 - [31] E. Engel and S. H. Vosko, *Phys. Rev. A* **47**, 2800 (1993).
 - [32] T. Kirchner, M. Horbatsch, H. J. Lüdde, and R. M. Dreizler, *Phys. Rev. A* **62**, 042704 (2000).
 - [33] H. J. Lüdde and R. M. Dreizler, *J. Phys. B* **18**, 107 (1985).
 - [34] M. Murakami, T. Kirchner, M. Horbatsch, and H. J. Lüdde, *Phys. Rev. A* **85**, 052704 (2012).
 - [35] M. E. Rudd, T. V. Goffe, and A. Itoh, *Phys. Rev. A* **32**, 2128 (1985).
 - [36] R. D. DuBois, *Phys. Rev. A* **36**, 2585 (1987).
 - [37] J. H. McGuire, *Electron Correlation Dynamics in Atomic Collisions* (Cambridge University Press, Cambridge, UK, 1997).

- [38] I. Dmitriev, Y. Teplova, and Y. Fainberg, *J. Exp. Theor. Phys.* **89**, 830 (1999).
- [39] J.-Y. Chesnel, H. Merabet, X. Husson, F. Frémont, D. Lecler, H. Jouin, C. Harel, and N. Stolterfoht, *Phys. Rev. A* **53**, 2337 (1996).
- [40] S. H. Be, T. Tonuma, H. Kumagai, H. Shibata, H. Kase, T. Kambara, I. Kohno, and H. Tawara, *J. Phys. B* **19**, 1771 (1986).
- [41] T. Kirchner, M. Horbatsch, and H. J. Lüdde, *Phys. Rev. A* **66**, 052719 (2002).
- [42] M. Murakami, T. Kirchner, M. Horbatsch, and H. J. Lüdde, *Phys. Rev. A* **85**, 052713 (2012).
- [43] M. Keim, A. Achenbach, H. J. Lüdde, and T. Kirchner, *Phys. Rev. A* **67**, 062711 (2003).
- [44] M. Baxter and T. Kirchner, *Phys. Rev. A* **87**, 062507 (2013).